RSC Advances

ROYAL SOCIETY OF CHEMISTRY

www.rsc.org/advances

‘

Thermodynamics of native defects in In_2O_3 crystal with first-principles method*

Jian Liu, Tingyu Liu**[1], Fengming Liu, Haixin Li

College of Science, University of Shanghai for Science and Technology, 516 Jungong Road, Shanghai 200093, P.R. China

Abstract

The stability of the intrinsic point defects in bixbyite In_2O_3, including oxygen vacancies, oxygen interstitials, indium vacancies and indium interstitials, under a range of temperatures, oxygen partial pressures and stoichiometries has been studied by the computational method. The calculated results indicate that the a-position is not a suitable site for interstitials and both b-position and d-position are favorable for indium vacancies with the similar defect formation energies. Both donors (oxygen vacancies and indium interstitials in c-position) and acceptors (indium vacancies in b/d-position and oxygen interstitials in c-position) are predicted having shallow defect transition levels. Then defect formation energies of all possible charged states are used in thermodynamic calculations to predict the influence of temperature and oxygen partial pressure and varied Fermi level in limited area on the relative stabilities of the point defects. The combined formation energies of point defect complexes, including Frenkel pairs,

*This work is supported by the Hujiang Foundation of China (A14001)
**Corresponding author. Tel: 086-021-65667034.
E-mail address: liutyyxj@163.com (T.Y. Liu)

‘

anti-Frenkel pairs and Schottky pairs, are calculated to predict relative stability in the paper.

Keywords: First-principles; In_2O_3; Intrinsic point defects, Thermodynamics

1. Introduction

Indium oxide (In_2O_3) is a wide band gap transparent conducting oxide (TCO) which is attracting a great deal of attention because of its high electrical conductivity, high optical transparency in the visible region, and high reflectivity in the infrared [1,2]. Bixbyite In_2O_3 is currently used in a wide range of optoelectronic applications, light-emitting diodes (OLEDs) [3] including flat-panel displays, and solar cells. In addition, In_2O_3 is a suitable material for gas sensing applications especially of ozone and oxygen [4].

The electron concentration and conductivity in n-type In_2O_3 have been studied experimentally since the 1970s [5-7]. It has been well concluded that the intrinsic defect contributes to the pronounced non-stoicheiometry which results in n-type semiconductivity [6]. Experimental techniques, such as thermogravimetric and conductivity measurements, have long been used to determine the deviation from non-stoicheiometry in In_2O_3 as a function of temperature and oxygen partial pressure. From the experimental point of view, both the nonstoichiometry and the n-type conductivity have been assigned to doubly charged oxygen vacancies [5].

Further research about anion vacancies in In_2O_3 was discussed [8]. Lany and Zunger

presented that conductivity should originate from a photo-induced process: the oxygen vacancy acts as color center binding two electrons [9]. Gan and Lu et al. further demonstrated that oxygen vacancies promoting photoelectrochemical performance of In_2O_3 nanocubes [10]. In addition, it is confirmed that oxygen vacancies can quantitatively account for the rather moderate conductivity in thin films surface [11]. From above, it is mostly implied that the native donor oxygen vacancies is the origin of the conductivity.

On the contrary, it is concluded that the origin of the native donor in undoped In_2O_3 is interstitial indium, but with the coexistence of V_O. Interstitial indium can generate a shallow donor level, close to the conduction band, and an even shallower donor level is formed when it associates with an oxygen vacancy [12]. V_O cannot generate free electrons by itself, but can facilitate emergence of the donor In_i [12].

In the case of In_2O_3, several DFT studies have been applied to examine defect structures and stabilities. These studies have focused on, for example, Frenkel or oxygen vacancies and indium interstitials defect complexes [12,13], extrinsic point defects [14,15] and the electronic structures of intrinsic point defects [16]. Recent calculations of intrinsic defect formation energies (DFE) in In_2O_3 [17] find that oxygen vacancies are the predominant point defect under indium-rich conditions and oxygen dumbbell interstitials are the predominant point defect under oxygen-rich conditions. However, these studies have been restricted to special conditions of oxygen rich or meal rich limit. In addition, none of these studies address the relative stabilities of intrinsic point defect under varied

‘

experiment conditions, such as temperature and partial oxygen pressure.

In present paper, quantitative predictions of the stabilities of charged intrinsic point defects in Bixbyite In_2O_3 have been performed using a combination of ab initio and thermodynamic calculation. We have performed the calculations on the basis of density of theory (DFT) using the GGA+U method to achieve a better description of the structure of the material. In particular, DFT calculations are used to study the structure and active sites about both perfect and defective crystal. This information is then used to determine DFEs. Importantly, a quantitative link is made to temperature and oxygen partial pressure and Fermi level, which are the key parameters for controlling the type and concentration of dominant defects in In_2O_3. The resulting self-consistent set of DFEs are not only necessary for predicting bulk point defect chemistry, but also are crucial input parameters for equilibrium, space-charge segregation models that can predict the equilibration of point with higher dimensional defects such as surfaces and grain boundaries.

2. Computational methods

2.1. Electronic structure computational

Density functional theory (DFT) calculations are all performed using Vienna ab initio simulation package (VASP) [18,19]. Electron-ion interactions are treated using projector augmented wave (PAW) method [20,21]. The generalized gradient approximation (GGA) in the parameterization by Perdew, Burke and Ernzerhof (PBE) [22] was selected to express the exchange-correlation potential. The electron wavefunctions are described using a plane-wave basis set with a cut-off energy of 500 eV [17]. It is

‘

proved to be sufficient for defect calculations. The valence electrons for indium are generated in $4d^{10}5s^{2}5p^{1}$ configuration and those for oxygen are in the $2s^{2}2p^{4}$ configuration. Since the ‘standard’ GGA functional underestimates the binding energy of In 4d electrons, which leads to a considerable overestimation of the O $2p^{4}$-In $4d^{10}$ hybridization. Therefore we adopted the GGA+U method in the formulation by Dudarev et al [23] with U−J=7 eV [17,24]. This method has been successfully used in a recent study of the valence band structure of In_2O_3 [24]. The Brillouin-zone integrations are carried out using the Monkhorst-Pack scheme with a k-mesh of 3×3×3 points, which proved to be sufficient for the defect calculation.

The defect calculations are carried out with fixed cell parameters as obtained for the ideal structure while the maximum force is converged to less than 10 meV $Å^{-1}$. In_2O_3 (bixbyite) has the Symmetry point groups $Ia\bar{3}$, space number 206 and lattice parameter a=10.117 Å. The calculations are carried out of a suppercell with 80 atoms. Figure 1 shows the possible sites for interstitials and vacancies. Here, the calculated band gap of In_2O_3 is 1.79 eV, which is close to the experiment values [31].

2.2. Defect formation energies

The Gibbs free energy for point defect formation in In_2O_3 is given by a function of defect species α, charge state q, oxygen partial pressure P and temperature T [25,26].

$$\Delta G_{\mathrm{f}}(\alpha,q,T,P) \cong E^{\mathrm{total}}(\alpha,q) - E^{\mathrm{total}}(\mathrm{perfect}) + \Delta n_i \mu_i(T,P) + q(E_{\mathrm{VBM}} + E_{\mathrm{F}} + \Delta V) - T\Delta S(T,V_0) \quad (1)$$

Where $\Delta G_f(\alpha,q,T,P)$ is the defect formation energy. $E^{\mathrm{total}}(\alpha,q)$ is the relaxed total energy of

supercell including the defect α of charge state q obtained from the DFT calculations, and E^{total}(perfect) is the relaxed total energy of the corresponding ideal supercell crystal also obtained from DFT calculations. Δn_i denotes the change of the number of atoms of type i from the ideal to defective crystal. For example, $\Delta n_i = \Delta n_O = -1$ for an oxygen interstitial, and $\Delta n_i = \Delta n_{In} = 1$ for an indium vacancy. $\mu_i(T,P)$ is the chemical potential of the defect atom i as a function of temperature and oxygen partial pressure, which is obtained from combination of DFE and thermodynamic calculations. E_{VBM} is the maximum of valence-band, and ΔV is the correction based on Potential alignment correction method between ideal cell and defected crystal [32]. E_F is the Fermi level which varied from 0 eV to band gap. V_0 is crystal volume which is constant in calculation. Lastly, ΔS is the vibrational entropy which is caltulated from vasp.

2.3.Thermodynamic component

Chemical potential $\mu_i(T,P)$ is determined by the system environment. Oxygen chemical potential [27,28] is calculated as follows:

$$\mu_O(T,P) = \frac{1}{3}[\mu^0_{In_2O_3} - 2\mu^0_{In} - \Delta G^0_{f,In_2O_3}] + \Delta\mu^0_O(T) + \frac{1}{2}k_B T \ln(\frac{P}{P^0}) \quad (2)$$

In this field, $\mu^0_{In_2O_3}$ and μ^0_{In} are the chemical potential of In_2O_3 and In, which are calculated with VASP code, respectively. While $\Delta G^0_{f,In2O3}$ is the Gibbs formation energy per mole in the standard state obtained from standard thermodynamic data [29]. $\Delta\mu^0_O$(T) is the difference chemical potential of oxygen between any temperature and standard

temperature gained from thermodynamic data [30]. Combining Eq. (1) and (2), we can get defect formation energies under different temperature and oxygen partial pressure. Table 1 shows a comparison of oxygen chemical potential, which calculated from Eq. (2) and the defect formation energies for oxygen vacancies of +1 and +2 charges under different temperatures and oxygen partial pressures. This comparison indicates that temperature and oxygen partial pressure all play an important role, which should not be ignored in defect formation calculations.

3. Results and discussion

3.1 Charge transfers and band gap corrections

Figure 2 shows the calculation results of the defect transition level for oxygen vacancy, indium interstitial on c and a sites ($In_{i\text{-}c}$, $In_{i\text{-}a}$), oxygen interstitial on c and a sites ($O_{i\text{-}c}$, $O_{i\text{-}a}$), indium vacancy on b and d sites ($V_{In\text{-}b}$, $V_{In\text{-}d}$). The results indicate that both donors and acceptors have shallow defect transition levels except for high ionized defects, such as $In_{i\text{-}c}^{\cdots}/In_{i\text{-}c}^{\cdot\cdot}$ and $O_{i\text{-}c}^{''}/O_{i\text{-}c}^{'}$, which manifests that both donors and acceptors are prefer to remain in low ionized or neutral charge state. These shallow levels further indicate that the thermodynamic transitions are easily activated.

Usually, all the calculated transition levels that are scaled by the ratio of the experimental to the calculated data of the band gap using the scissor operator. This correction is only applied on conduction states and the DFEs of donors increased by an energy equal of the difference in one particle energies times the occupation of the corresponding defect levels. The choice to only correct the conduction band, however, is

usually not justified, and furthermore the change in energy does not include defect level relaxation and the double counting correction term using this scheme [17]. So the transition levels correction is omitted in this work.

3.2. Sites for vacancies and interstitials

Within the bixbyite lattice there are four distinct defect sites: a, c, b and d sites. The a-position and c-position are usually referred to as the structural vacancy sites, while b-position and d-position are acted as the structural interstitial sites (Fig. 1). The DFEs of interstitial in a-position is always much higher than that in c-position for both indium and oxygen interstitial. So the c-position is most favorable for indium (In_{i-c}) and oxygen interstitial (O_{i-c}) and a-position is not a suitable interstitial site although the temperature and oxygen partial pressure varied. However, the b-position and d-position are both favorable for indium vacancy as the defect formation energy are much closed to each other. The DFEs of indium vacancy in d-position is a little lower than in b-position when Fermi level varied from 0 eV to 0.85 eV and a reverse phenomenon is found when Fermi level position locates in the 0.85-2.8 eV region.

3.3.Defect formation energy

The calculation of predicting defect formation energies may be used to obtain defect concentrations and well predict doping behavior. Therefore, the defect formation energy of different charged defects are calculated using our approach as a function of system conditions. Figure 3a-c shows the calculated DFEs of V_{In-b}, V_{In-d}, In_{i-b}, In_{i-d}, V_O, O_{i-c} and

‘

$O_{i\text{-}a}$ in pure In_2O_3 as a function of Fermi level E_F under reducing conditions ($\log(P_{O2}/P^0)$=-10) at three different temperatures. The factual Fermi level of In_2O_3 is varied by dopants or impurities, in addition to the system temperature (T) and oxygen partial pressure (P_{O2}). It is therefore necessary to determine the DFEs over a physically reasonable range of Fermi energies to increase the correlation of the calculated values. So the Fermi level of all possible values is considered here.

When the Fermi level varies from 0 to 2.8 eV at room temperature and low oxygen partial pressure, the most stable intrinsic point defects are shown to be $V_O^{\cdot\cdot}$, $O_{i\text{-}c}^{''}$ and $V_{In\text{-}b}^{'''}$, respectively (see Fig. 3a). In contrast, when the Fermi level is approximately equal to $E_g/2$ at room temperature, the stable charge states for these same point defects are $V_O^{\cdot\cdot}$, $O_{i\text{-}c}^{''}$, $V_{In\text{-}b}^{'''}$ and $In_{i\text{-}c}^{\cdot\cdot\cdot}$. The results also show that, as the Fermi level decreases, the thermodynamically preferred charge states of the indium interstitials change from neutral to +1, +2 and +3. Intriguingly, the p-type defect $O_{i\text{-}c}^{''}$ and $V_{In\text{-}b}^{'''}$ are predicted to be the most stable under conditions of Fermi level E_F=1.3-2.8 eV, T=300 K and $P_{O2}=10^{-10}$ atm. While n-type behavior always be find when experimental measurements are normally carried on In_2O_3 [5-7].

Over almost the full range of Fermi levels considered here, oxygen vacancies of various charge states are predicted to be the most stable intrinsic defect in In_2O_3 at high temperature, except at very high Fermi levels.

The most stable intrinsic defect as a function of Fermi level, oxygen partial pressure and temperature are determined in the three-dimensional defect formation energy

diagrams which are divided into three regions (Fig. 4). The graph shows the most stable point defect is oxygen vacancies when the external environment is located in the region 1. When E_F is in the range of 0-1.66 eV, 1.66-2 eV and 2-2.8 eV, the oxygen vacancies of +2, +1 and 0 charge states are predicted to be the most stable intrinsic defect in the region 1, respectively. The most stable point defect has a transfer to oxygen interstitials and indium vacancies when the experimental environment fit to the region 2 and region 3, respectively. The most stable point defects of oxygen interstitials change from -1 to -2 charge state in region 2 when E_F changes from 1.26 to 2.8eV and the most stable point defects of indium vacancies maintain -3 charge state in whole region 3. And, intriguingly, when E_F is less than 1.05 eV, the most stable intrinsic defect is always $V_O^{\cdot\cdot}$ despite the temperature and oxygen partial pressure varying in Fig. 4.

Figure 5 shows two-dimensional defect formation scheme as a function of temperature and oxygen partial pressure with the E_F = 1.4 eV, 2.4 eV respectively. Figure 5a (E_F = 1.4 eV) show that the ordering of most stable defects are oxygen interstitials → oxygen vacancies with the temperature increases and partial pressure decreases (going from bottom right to top left in each figure). In addition, Figure 5b (E_F = 2.4 eV) show the ordering of most stable defects are indium vacancies → oxygen interstitials → oxygen vacancies. The predicted preferred defects with different Fermi levels are disparate, although it has the same temperature and oxygen partial pressure. For example, $O_{i\text{-}c}^{''}$ and $V_{In\text{-}b}^{'''}$ are predicted to be the most stable intrinsic defects in the low temperature region with the E_F=1.4, 2.4 eV respectively, whereas, $V_O^{\cdot\cdot}$ and V_O^{x} are predicted to be the most stable

intrinsic defects in the region of high temperature and reduced conditions.

The most stable charge states and corresponding formation energies of distinct intrinsic point defects in In_2O_3 at three typical conditions are listed in Table 2. Since it is unconcern the equilibrium concerntration of defects or inpurities can be achieved for any experimental conditions which have an influence on fermi energy. Therefore, it is significant to computer all possible charge states under different external experiment and explore the relative stabilities of point defects in indium oxide.

In the preceding discussion, the relative stabilities of individual defects are considered and discussed. However, point defects do not occur alone but as part of charge-neutral complexes. The DFEs of Frenkel, anti-Frenkel and Schottky defect complexes are therefore also calculated using the following equations:

$$\Delta G_{\mathrm{f}}^{\mathrm{F}} = E^{\mathrm{total}}(V_{\mathrm{In}},-q) - E^{\mathrm{total}}(\mathrm{perfect}) + E^{\mathrm{total}}(\mathrm{In_i},q) - E^{\mathrm{total}}(\mathrm{perfect}) - T(\Delta S_{\mathrm{V_{In}}}(\mathrm{T,V}) + \Delta S_{\mathrm{In_i}}(\mathrm{T,V})) \quad (3)$$

$$\Delta G_{\mathrm{f}}^{\mathrm{AF}} = E^{\mathrm{total}}(\mathrm{V_O},q) - E^{\mathrm{total}}(\mathrm{perfect}) + E^{\mathrm{total}}(\mathrm{O_i},-q) - E^{\mathrm{total}}(\mathrm{perfect}) - T(\Delta S_{\mathrm{V_O}}(\mathrm{T,V}) + \Delta S_{\mathrm{O_i}}(\mathrm{T,V})) \quad (4)$$

$$\Delta G_{\mathrm{f}}^{\mathrm{S}} = 2(E^{\mathrm{total}}(\mathrm{V_{In}},-3q) - E^{\mathrm{total}}(\mathrm{perfect})) + 3(E^{\mathrm{total}}(\mathrm{V_O},2q) - E^{\mathrm{total}}(\mathrm{perfect})) + 2\mu_{\mathrm{In}} + 3\mu_{\mathrm{O}} - T(2S_{\mathrm{V_{In}}}(\mathrm{T,V}) + 3S_{\mathrm{V_O}}(\mathrm{T,V})) \quad (5)$$

The definitions of $E^{\mathrm{total}}(\alpha,q)$ and $E^{\mathrm{total}}(\mathrm{perfect})$ are the same as in Eq.(1)

These defect complexes are treated as a combination of charged or neutral defects and the total charge states of the defect complex is neutral. For instance, four different types of Frenkel pair modes are considered: $V_{In}^{x}+In_i^{x}$, $V_{In}^{'}+In_i^{\cdot}$, $V_{In}^{''}+In_i^{\cdot\cdot}$ and $V_{In}^{'''}+In_i^{\cdot\cdot\cdot}$. Similar combination is considered for anti-Frenkel and Schottky pairs. A nice feature of

‘

Analysis of the defect complexes is that, since the defect complexes are charge neutral, the calculations doesn’t consider the Fermi level, as the formation energy form a transverse line in Fig. 6.

The two more stable types Frenkel pairs including $V_{In\text{-}b}$+$In_{i\text{-}c}$ and $V_{In\text{-}d}$+$In_{i\text{-}c}$ compared with other Frenkel pairs are shown in the Figure 6a. The most stable Frenkel pair is $V_{In\text{-}b}^{'''}$+$In_{i\text{-}c}^{\cdot\cdot\cdot}$ and $V_{In\text{-}d}^{'''}$+$In_{i\text{-}c}^{\cdot\cdot\cdot}$ combination is also stable since its DFE is only a little higher than the former’s about 0.1eV.

From the Figure 6b, it can be seen that all the DFEs of anti-Frenkel pairs are lower than that of Frenkel pairs. The combination of V_O+$O_{i\text{-}c}$ is more stable than V_O+$O_{i\text{-}a}$ for any charged state, which is well agreement with the fore-discussion that a-position is not a suitable interstitial site.

From Figure 6a and b, it can be concluded that charged defect pairs have lower DFEs. For instance, the combination $V_O^{\cdot\cdot}$+$O_{i\text{-}c}^{''}$($V_{In\text{-}b}^{'''}$+$In_{i\text{-}c}^{\cdot\cdot\cdot}$) has a lower DFE. The anti-Frenkel pair is more stable than the Frenkel pair. In addition, the DFEs of Schottky pairs is much higher than that of Frenkel and Anti-Frenkel pairs. Therefore anti-Frenkel pairs are the most stable and Schottky pairs are lowest thermodynamically stable. However, Aron believes that the DFEs of the anti-Frenkel pair is moderately higher than that of the Schottky defect energy, nevertheless, it is still lower than that of the Frenkel pair[13]. The reason to the argument is that their calculation formula of the DFEs has some difference from ours.

‘

Conclusions

In summary, the native point defects have been studied at varied temperature and confined oxygen partial pressure in In_2O_3 using ab initio methods based on the GGA+U formalism. As to the In_2O_3 structural, we find the c-position is the favorable interstitial site and b/d-position has same role for indium vacancies with similar DEFs. It indicates that oxygen vacancies is the most stable point defect in n-type behavior and indium vacancies or oxygen interstitials is the most stable defect in p-type behavior. In addition, as to defect complexes, we conclude that anti-Frenkel pairs is most thermodynamic stable than Frenkel pairs and Schottky pairs and charged defect complexes are more likely to occur, such as $V_O^{\cdot\cdot}+O_{i\text{-}c}^{''}$. Of considering key parameters to calculate defect formation energy, it is therefore generally applicable for the systematic evaluation of defect formation in electronic ceramics under the full range of temperature and atmospheric conditions, such as are important for catalysis (low temperature, high pressure) and gas sensing (high temperature, low pressure) applications.

Reference

[1] R.G. Gorden , MRS. Bulletin, 2000, 25, 52-57.

[2] H. Hartnagel, A.L. Dawar, A.K. Jain, C. Jagadish, Institute of Physics Pub., England,1995.

[3] L.S. Hung, C.H. Chen, Mater. Sci. Eng. R Rep., 2002, 39, 143-222.

‘

[4] V. Golovanov, M.A. Mäki-Jaskari, T.T. Rantala, G. Korotcenkov, V. Brinzari, A. Cornet, J. Morante, Sens. Actuators B: Chem., 2005, 106, 563-571.

[5] J.H.W. De Wit, G. Van Unen, M. Lahey, J. Phys. Chem. Solids, 1977, 38, 819-824.

[6] J.H.W. D. Wit, J. Solid State Chem., 1975 13, 192-200.

[7] J.H.W. D. Wit, J. Solid State Chem., 1973, 8, 142-149.

[8] I. Tanaka, K. Tatsumi, M. Nakano, H. Adachi, JACS., 2002, 85, 68-74.

[9] S. Lany, A. Zunger, Phys. Rev. Lett., 2007, 98, 045501.

[10] J. Gan, X. Lu, J. Wu, S. Xie, T. Zhai, M. Yu, Z. Zhang, Y. Mao, S.C.I Wang, Y. Shen, Y. Tong, Sci. Rep., 2013, 3.

[11] S. Lany, A. Zakutayev, T.O. Mason, J.F. Wager, K.R. Poeppelmeier, J.D. Perkins, J.J. Berry, D.S. Ginley, A. Zunger, Phys. Rev. Lett., 2012, 108, 016802.

[12] T. Tomita, K. Yamashita, Y. Hayafuji, H. Adachi, Appl. Phys. Lett., 2005, 87, 051911.

[13] A. Walsh, C.R.A. Catlow, A.A. Sokol, S.M. Woodley, Chem. Mater., 2009, 21, 4962-4969.

[14] O. Warschkow, D.E. Ellis, G.B. González, T.O. Mason, JACS., 2003, 86, 1707-1711.

[15] T.O. Mason, G.B. Gonzalez, D.R. Kammler, N. Mansourian-Hadavi, B.J. Ingram, Thin Solid Films, 2002, 411, 106-114.

[16] O. Warschkow, D.E. Ellis, G.B. González, T.O. Mason, JACS., 2003, 86, 1700-1706.

‘

[17] P. Ágoston, P. Erhart, A. Klein, K. Albe, J. Phys.: Condens. Matter, 2009, 21, 455801.

[18] G. Kresse, J. Furthmüller, Phys. Rev. B, 1996, 54, 11169.

[19] G. Kresse, J. Furthmüller, Comput. Mater. Sci., 1996, 6, 15-50.

[20] P.E. Blöchl, Phys. Rev. B, 1994, 50, 17953.

[21] G. Kresse, D. Joubert, Phys. Rev. B, 1999, 59, 1758-1775.

[22] J.P. Perdew, K. Burke, Phys. Rev. Lett., 1996, 77, 3865-3868.

[23] S.L. Dudarev, G.A. Botton, S.Y. Savrasov, C.J Humphreys, A.P. Sutton, Phys. Rev. B, 1998, 57, 1505-1509.

[24] P. Erhart, A. Klein, Phys. Rev. B, 2007, 75, 153205.

[25] S.B. Zhang, J.E. Northrup, Phys. Rev. Lett., 1991, 67, 2339-2342.

[26] G.X. Qian, R.M. Martin, D.J. Chadi, Phys. Rev. B, 1988, 38, 7649-7663.

[27] I.G. Batyrev, A. Alavi, M.W. Finnis, Phys. Rev. B, 2000, 62, 4698-4706.

[28] M.W. Finnis, A.Y. Lozovoi, A. Alavi, The oxidation of NiAl: What can we learn from ab initio calculations?, Annu. Rev. Mater. Res., 2005, 35, 167.

[29] W.M. Haynes, D.R. Lide, Handbook of chemistry and physics, C.R.C. Press, New York, 2010.

[30] NIST. NIST Chemistry WebBook. NIST, 2005.

[31] A. Klein, Appl. Surf. Sci., 2000, 77, 2009-2011.

[32]J. Lee, S. Han, PCCP, 2013, 15, 18906-18914.

‘

‘

Figure caption:

Fig. 1. Arrangement of atoms in In_2O_3. b and d site represent possible vacancy site for Indium atoms. Oxygen vacancy may locate on e site. a and c site are the interstitial site for indium or oxygen atoms.

Fig. 2. Calculated defect transition levels ε(defect$^{q1/q2}$) for the major defects. The circles below and above the transition levels denote the occupancy of the corresponding defect charge state. The experiment band gap value is 2.8 eV [31].

Fig. 3. Calculated DFE of point defects (V_O, In_i, O_i and V_{In}) is a function of Fermi level, oxygen partial pressure and temperature (Fig. 3a-f). Figure 3a-c shows formation energies at different temperatures (T=300 K in (a), T=800 K in (b) and T=1400 K in (c) in the reduced state ($\log(P_{O2}/P^0)$=-10). Figure 3d-f shows formation energy at different temperatures (T=300 K in (d) ,T=800 K in (e) and T=1400 K in (f) in the near-neutral state ($\log(P_{O2}/P^0)$=-2).

Fig. 4. Three-dimensional defect formation scheme as a function of temperature, Fermi level and oxygen partial pressure. The space in graph is divided into three regions, region 1, region 2 and region 3.

Fig. 5. Two-dimensional defect formation scheme as a function of temperature and oxygen partial pressure calculated at two different Fermi level(E_F=1.4 eV in(a) and E_F=2.4 eV in (b), respectively).

Fig. 6. Calculated DFE of defect complexes at 1400K: (a) Frenkel pairs and (b) anti-Frenkel pairs. The DFEs of the complexes are compared with the DFEs of individual

‘

point defects at 1400K and oxygen pressures of ($\log(P_{O2}/P^0)$=-10). The formation energy of combination of charged indium vacancy and interstitial in b-position or in d-position is much closed. For example, $V''_{In\text{-}d/b}+In^{\cdot\cdot\cdot}_{i\text{-}c}$ means that the DFE of Frenkel $V''_{In\text{-}b}+In^{\cdot\cdot\cdot}_{i\text{-}c}$ is a little lower than that of the Frenkel $V''_{In\text{-}d}+ In^{\cdot\cdot\cdot}_{i\text{-}c}$.

‘

Table 1

Calculated oxygen chemical potential from Eq. (2) and defect formation energy from Eq. (1) for vacancies with +1 and +2 charges at various temperatures and oxygen partial pressures

T(K)	q	E_F(eV)	log(P/P^0)	μ(O)	qE_F(eV)	Sum of Eq. (1) (eV)
300	2	0	-2	-5.14	0.00	0.45
1400	2	0	-2	-6.70	0.00	-0.8
300	2	0	-10	-5.37	0.00	0.21
1400	2	0	-10	-7.81	0.00	-1.92
300	2	1.4	-2	-5.14	2.80	3.25
1400	2	1.4	-2	-6.70	2.80	2
300	2	1.4	-10	-5.37	2.80	3.01
1400	2	1.4	-10	-7.81	2.80	0.88
300	2	2.8	-2	-5.14	5.60	6.05
1400	2	2.8	-2	-6.70	5.60	4.8
300	2	2.8	-10	-5.37	5.60	5.81
1400	2	2.8	-10	-7.81	5.60	3.68
300	1	0	-2	-5.14	0.00	2.11
1400	1	0	-2	-6.70	0.00	0.86
300	1	0	-10	-5.37	0.00	1.87

1400	1	0	-10	-7.81	0.00	-0.26
300	1	1.4	-2	-5.14	1.40	3.51
1400	1	1.4	-2	-6.70	1.40	2.26
300	1	1.4	-10	-5.37	1.40	3.27
1400	1	1.4	-10	-7.81	1.40	1.14
300	1	2.8	-2	-5.14	2.80	4.91
1400	1	2.8	-2	-6.70	2.80	3.66
300	1	2.8	-10	-5.37	2.80	4.67
1400	1	2.8	-10	-7.81	2.80	2.54

‘

Table 2

Calculated defect formation energies for their most stable charge states of defects under three typical conditions: standard condition (T=300K, E_F=0.4eV，P_{O2}=1atm), reduced condition (T=1200K, E_F=1.4eV, P_{O2}=10^{-6}atm) and oxidized condition (T=700K, E_F=2.4eV, P_{O2}=10^{2}atm)

	standard condition		Reduced condition		Oxidized condition	
	charge	DFE(eV)	charge	DFE(eV)	charge	DFE(eV)
V_{In-b}	-1	4.87	-3	4.59	-3	-0.01
V_{In-d}	-1	4.81	-3	4.66	-3	0.06
V_O	+2	1.31	+2	1.77	0	3.97
In_{i-c}	+3	3.95	+3	4.32	+1	8.39
In_{i-a}	+3	4.56	+3	4.96	+1	8.88
O_{i-c}	0	3.31	-2	3.16	-2	0.18
O_{i-a}	0	3.77	-2	3.96	-2	0.98

‘

Figure 1

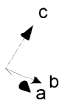

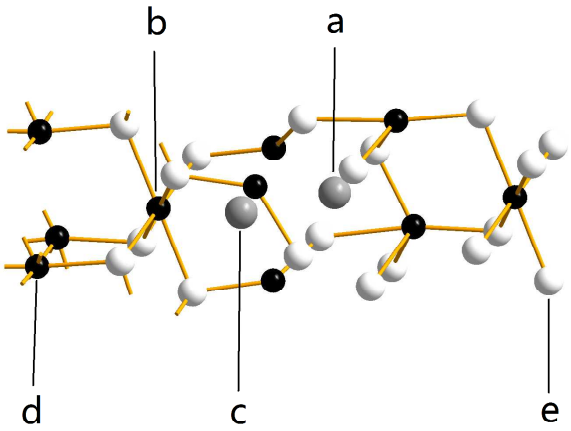

Figure 2

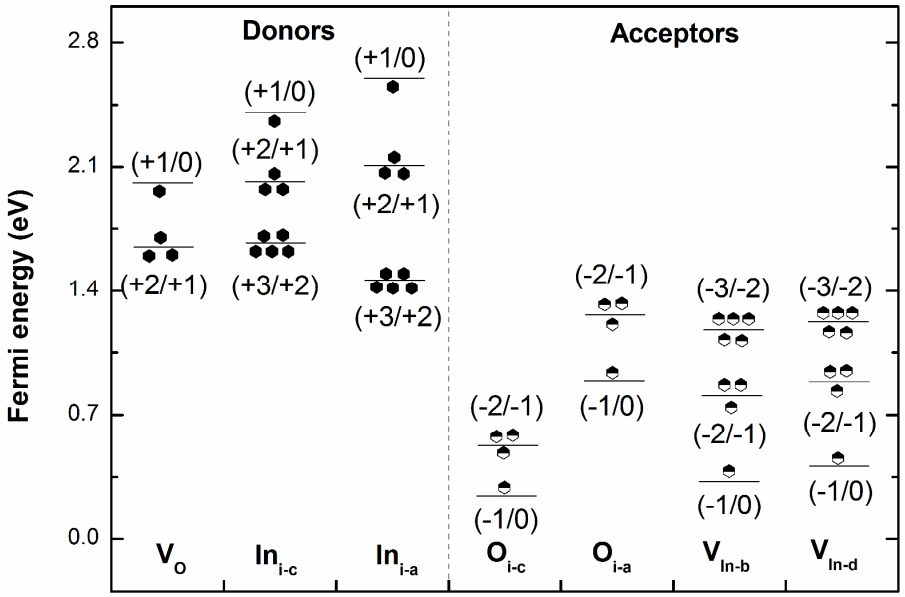

Figure 3a

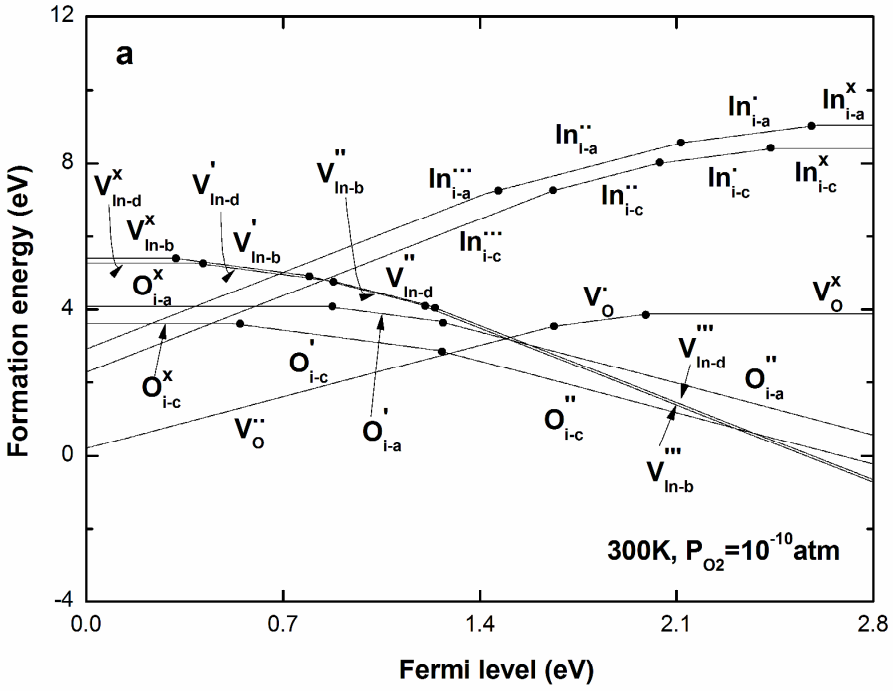

Figure 3b

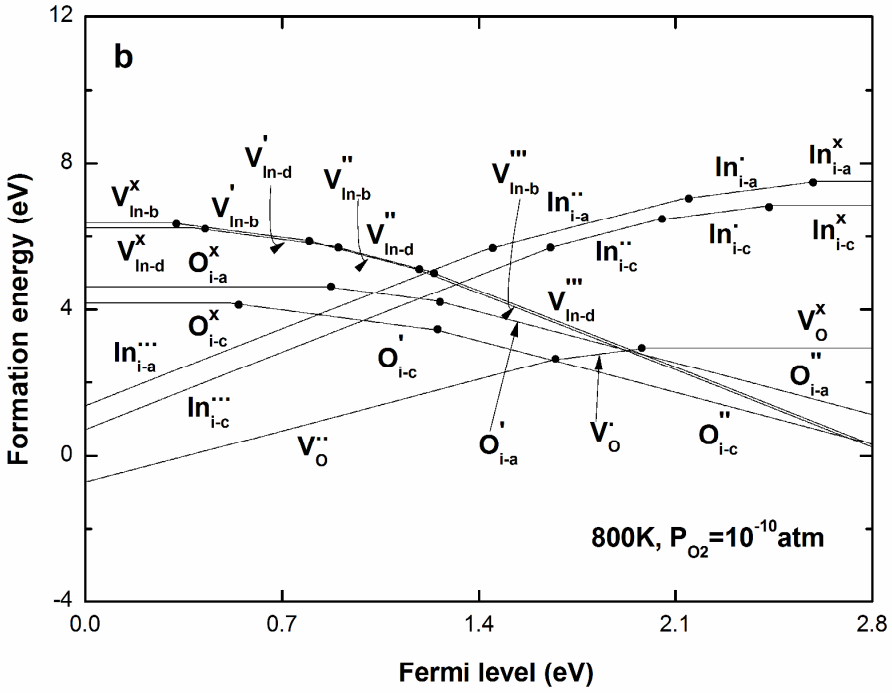

Figure 3c

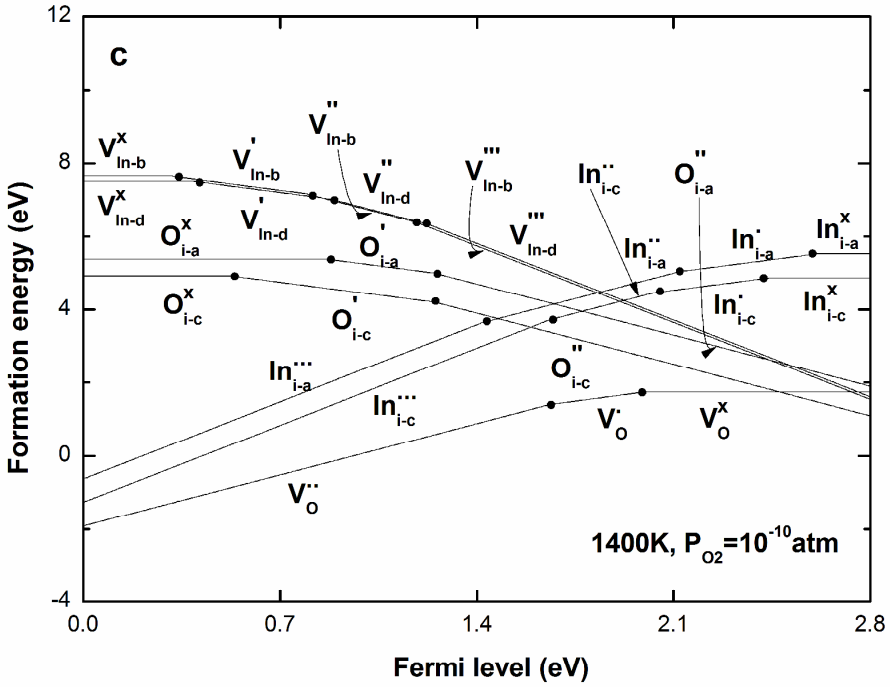

Figure 3d

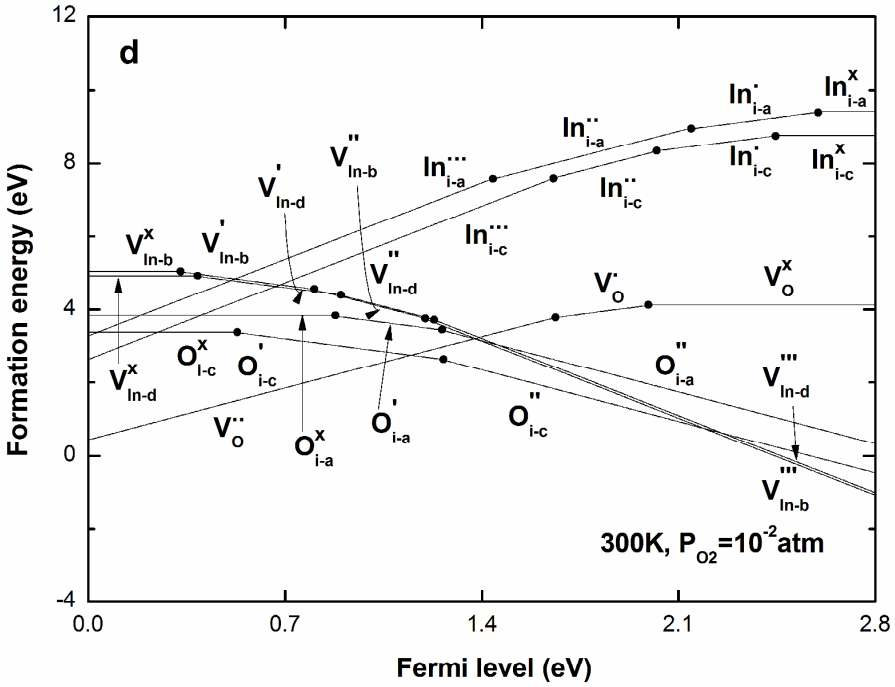

‘

Figure 3e

.

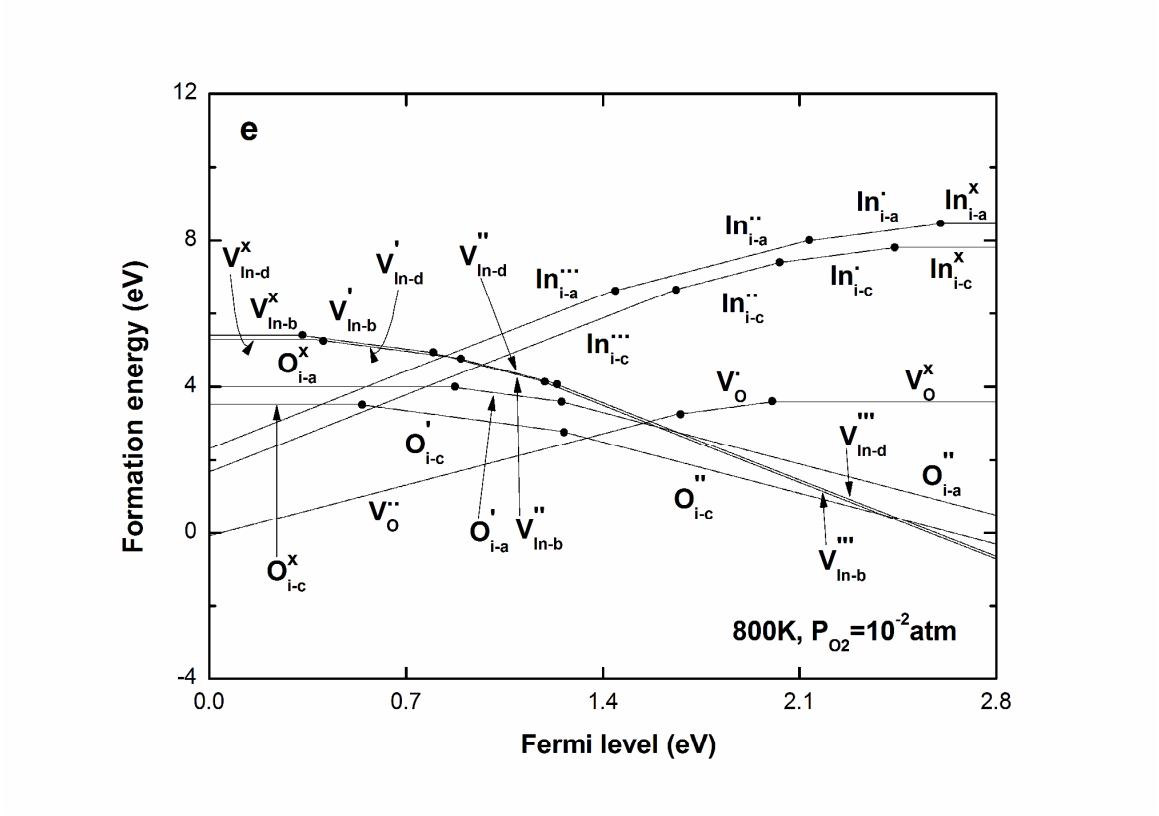

Figure 3f

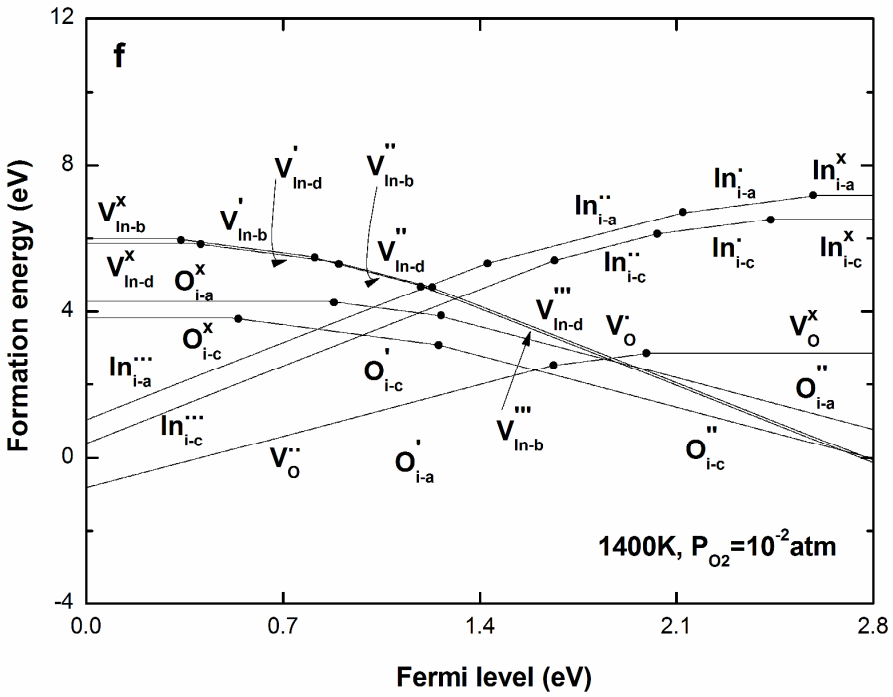

Figure 4

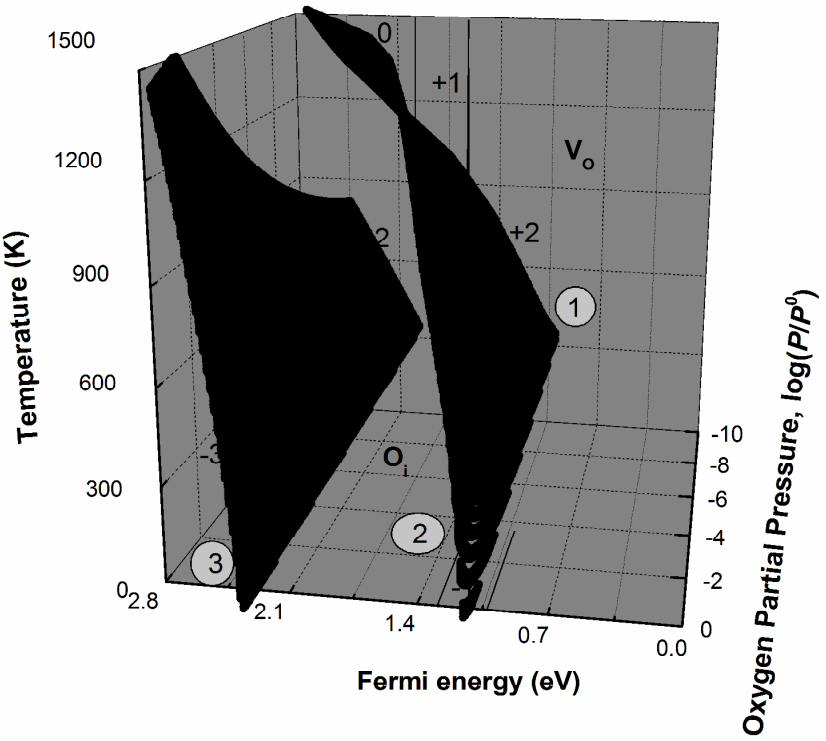

Figure 5a

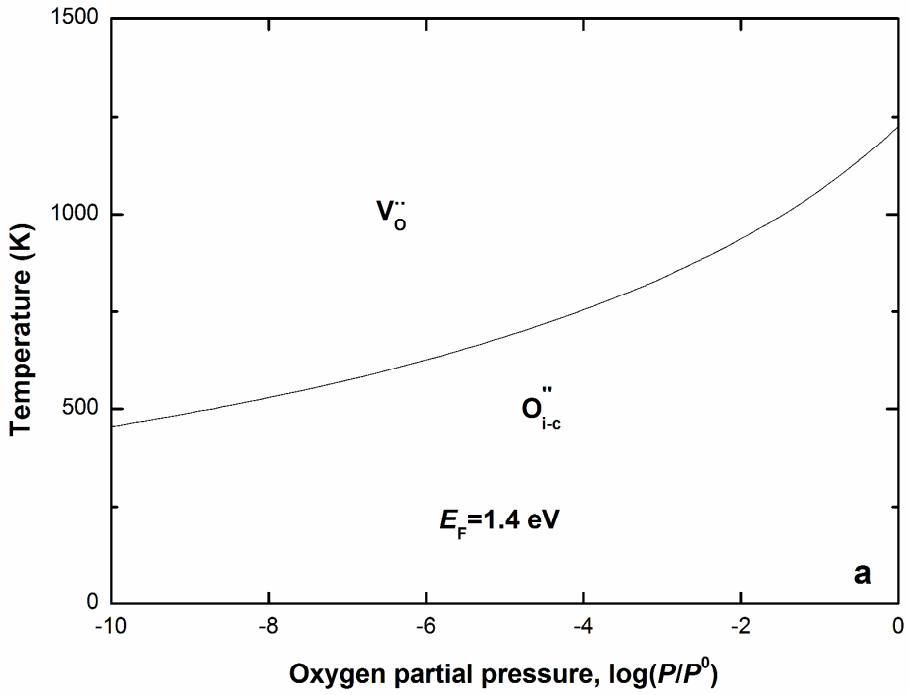

Figure 5b

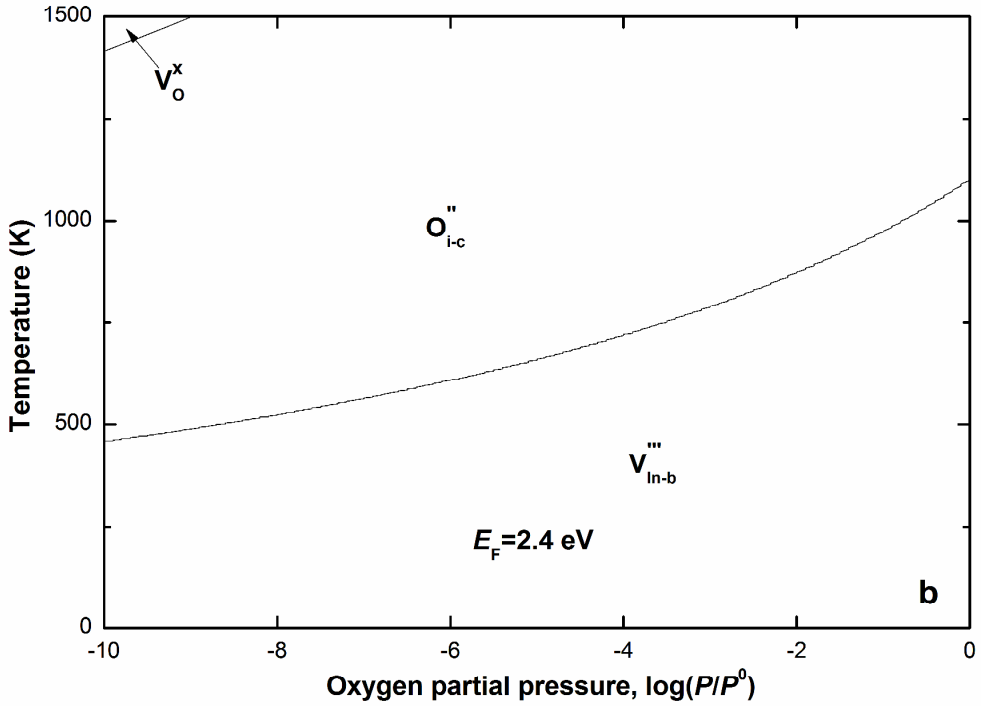

Figure 6a

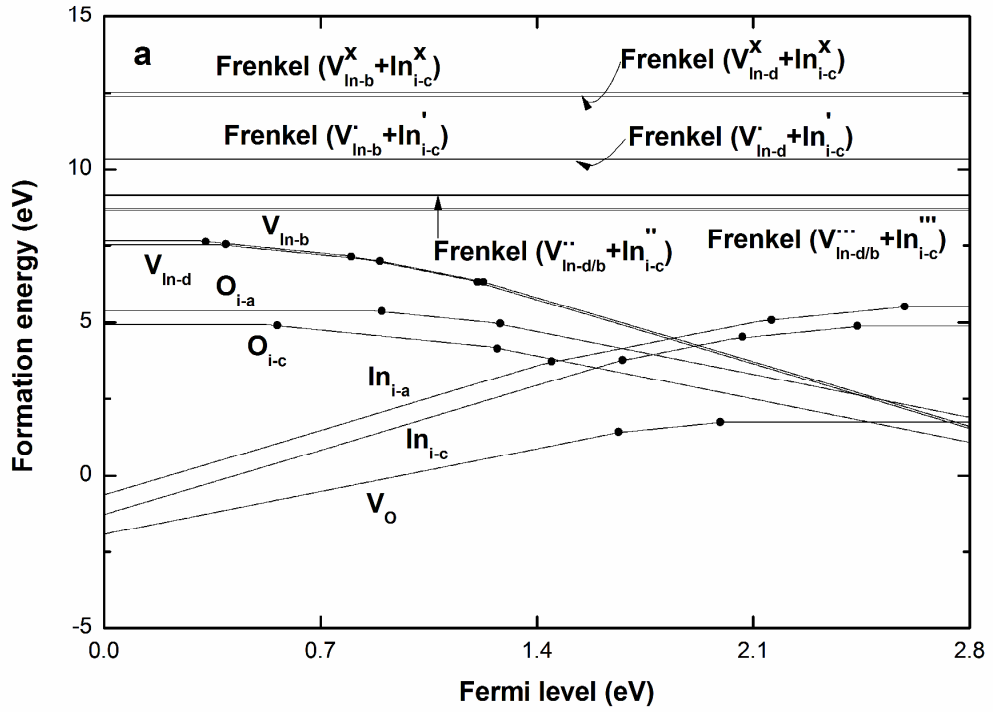

Figure 6b